ChemComm

COMMUNICATION

View Article Online
View Journal | View Issue

Cite this: *Chem. Commun.*, 2025, **61**, 15834

Received 22nd July 2025,
Accepted 27th August 2025

DOI: 10.1039/d5cc04144a

rsc.li/chemcomm

A direct comparison of lithium tetra(*n*-butyl) manganate(II) and magnesiate: structural insights and catalytic hydroamination of styrenes

Rebecca S. Jones,[a] Tobias Krämer,[b] Gary S. Nichol,[c] Mary F. Mahon,[a] Jon G. C. Kragskow[a] and Marina Uzelac*[a]

Previous studies have hinted at the similarities of Mn(II) and Mg alkyl complexes. Advancing this field, here we present a comparative study of tetra(*n*-butyl)lithium manganate(II) and magnesiate. Combining X-ray crystallographic studies, NMR characterisation and DFT calculations we disclose structural similarities and different nature of bonding which is ultimately reflected in enhanced reactivity of Mn(II) in hydroamination of styrenes.

Since the earliest reports on reactivity[1] and constitution[2] of organomanganese(II) complexes, these species displayed unique behaviour with their predominantly ionic Mn(II)–C bonds and disregard for the 18-electron rule. Despite displaying chemistry more comparable to organomagnesium reagents than to their neighbouring transition metals,[3] organomanganese(II) reagents suffer from reduced reactivity, tendency to undergo β-hydride elimination, and uncertain solution state characterisation due to their paramagnetic nature. Formation of bimetallic, synergic systems such as lithium manganates can enhance the reactivity and stability of these species. Thus, early studies by Girolami have shown alkyl complexes such as $[(TMEDA)_2Li_2MnR_4]$ (TMEDA = *N*,*N*,*N*′*N*′-tetramethylethylenediamine, R = ethyl, *n*-butyl) are stable towards β-hydride elimination at room temperature.[4] With regards to reactivity, Mulvey demonstrated the ability of $[(TMEDA)LiMn(TMP)(CH_2SiMe_3)_2]$ (TMP = 2,2,6,6-tetramethylpiperidide) to two-fold deprotonate ferrocene whereas $Mn(CH_2SiMe_3)_2$ is completely inert towards this substrate.[5] More recently, we have shown that tetraalkyl manganate $[(TMEDA)_2Li_2Mn(CH_2SiMe_3)_4]$ can enable direct and efficient Mn–I exchange of aryliodides, furnishing tetra(aryl) manganate intermediate that undergo spontaneous oxidative homocoupling at room temperature affording symmetrical bis(aryls).[6] Recently we have also shown how Girolami's butyl reagent $[(TMEDA)_2Li_2Mn^nBu_4]$ can effectively be used as a precursor for the synthesis of amidomanganates *via* direct amine deprotonation.[7]

Inspired by these precedents and with the aim of advancing the understanding on the similarities and differences between Mn(II) and Mg organometallics, here we report the synthesis and structural characterisation of tetra(*n*-butyl)lithium manganate and magnesiate as well as exploring their reactivity to act as pre-catalysts for hydroamination of styrenes. This synthetically valuable, atom efficient approach allows access to a wide range of amines. Various organometallic complexes across periodic table have been reported as efficient pre-catalysts in these transformations. Several magnesium catalysts showed activity in promoting intramolecular hydroamination, including bimetallic potassium magnesiate which efficiently catalyses intermolecular hydroamination of styrene.[8,9] While the use of Mn(I) complexes in catalytic hydroamination has been reported,[10] Mn(II) complexes remain virtually unexplored with only one study reporting the use of stoichiometric amounts of $MnBr_2$ in intramolecular hydroamination.[11]

Following Girolami's modified report,[4] salt-metathesis of $MnCl_2$ and ^{n}BuLi (1:4) in diethyl ether in the presence of 4 equivalents of TMEDA at 0 °C afforded a yellow suspension.[7] After solvent exchange and filtration of $[\{LiCl(TMEDA)\}_2]$, highly concentrated pentane solution was stored at −30 °C affording light yellow, X-ray quality crystals of $[(TMEDA)_2Li_2Mn^nBu_4]$ (**1**) (Fig. 1). To access the Mg analogue of **1**, we devised an alternative co-complexation approach[12] by reacting commercially available homoalkyls ^{n}BuLi, $^nBu_2Mg$ and TMEDA in a 2:1:2 ratio in hexanes. After stirring for 2 h at room temperature, and removal of volatiles, obtained white solid was recrystallised from pentane at −30 °C affording colourless, X-ray quality crystals of $[(TMEDA)_2Li_2Mg^nBu_4]$ (**2**).

The SC XRD study revealed **1** and **2** to be isomorphous adopting a lithium-rich, contacted ion-pair structure, known as "Weiss motif" (Fig. 1), isostructural with previously reported $[(TMEDA)_2Li_2MnR_4]$ (R = Me, Et, $CH_2CH_2{}^tBu$, CH_2SiMe_3)[4,6] and $[(TMEDA)_2Li_2MgR_4]$ (R = Me, CH_2SiMe_3)[13,14] species. Centrally

[a] *Department of Chemistry, University of Bath, Claverton Down, BA2 7AY, Bath, UK. E-mail: mu326@bath.ac.uk*
[b] *School of Chemistry, Trinity College Dublin, College Green, Dublin 2, Ireland*
[c] *School of Chemistry, University of Edinburgh, Kings Buildings, EH9 3FJ, Edinburgh, UK*

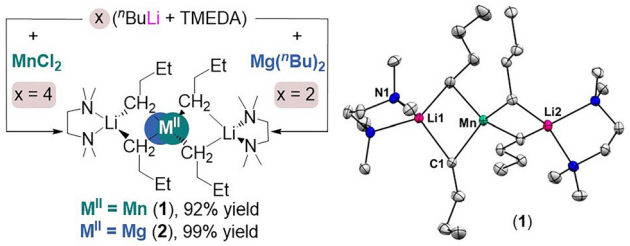

Fig. 1 Synthesis of isomorphous **1** and **2** (left) and molecular structure of **1** with thermal ellipsoids at 30% probability level and hydrogen atoms omitted for clarity (right).

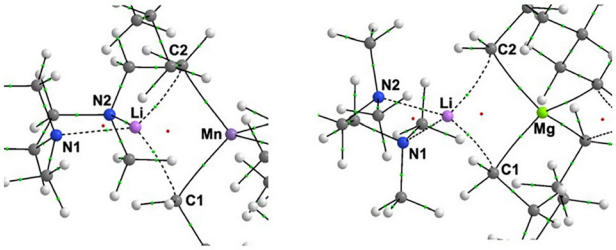

Fig. 2 Molecular graph for **1** (left) and **2** (right). BCPs (green dots) and RCPs (red dots) shown along with bond paths.

positioned M(II)-centre adopts marginally distorted tetrahedral geometry with a narrow range of angles [103.41(6)° to 113.87(6)° for Mn (**1**) and 104.26(5)° to 114.66(6)° for Mg (**2**)]. With only a slight difference in the covalent radii of Mg and Mn,[15] there is also very little variation in the M(II)–C bond lengths: 2.2358(14)–2.2671(14) Å in **1** and 2.2419(15)–2.2731(43) Å in **2**.

The four butyl groups form bridges to the outer, TMEDA-capped Li cations with the average Li–C bond distance of 2.254 Å and 2.234 Å for **1** and **2** respectively, consistent with Li–C(sp^3) contacts. Observed structural features support the existence of [$\{MBu_4\}^{2-}$] framework and Li-cations which engage in electrostatic interactions with α-carbanions of butyl ligands.

The Mn···Li distances of 2.582(2) and 2.575(2) Å are identical with those previously reported for other lithium manganates (Table S4) and indicate that there are no significant interactions between Li and Mn atoms. It is interesting to note however, that for all-carbon alkyl groups (Me, Et, ^{n}Bu, $CH_2CH_2{}^t$Bu) these distances are significantly shorter (approximately 10%) than the one found in the CH_2SiMe_3 version (see Table S4). The arrangement between the metals, determined by the Li···Mn···Li angle 166.67(7)° deviates from linearity, but fits the trend between the more bent structures containing smaller alkyls (Me, Et) and more linear structures with sterically more demanding alkyl groups (CH_2SiMe_3, $CH_2CH_2{}^t$Bu). The intermetallic arrangements of **1** are mirrored in **2** (see SI for full details). Methylene protons of bridging butyl ligands were located and independently refined however no M···HC_{Bu} contacts seem to be present, a picture further suggested by QTAIM analysis. With strikingly similar solid-state structures it is perhaps unsurprising that the solid-state IR spectra of **1** and **2** are also near identical (see SI for more details). Combination of C–C and C–H stretching, and C–H bending modes are visible in the 3050–2700 cm^{-1} region and are in good agreement with those reported by Girolami.[16]

The electronic structures of **1** and **2** were investigated by means of DFT calculations. The primary interaction found in the NBO analysis of **2** involves donation from the bridging carbanion lone pairs into the 3s acceptor orbital of Mg^{2+} ($E^{(2)}$ = 32.4 kcal mol^{-1}) combined with weaker donation into the 2s Li^+ orbital ($E^{(2)}$ = 5.9 kcal mol^{-1}). Topological analysis of the electron density using QTAIM places charges of +0.9*e*, +1.7*e* and −0.6*e* on Li, Mg and bridging carbon centres, respectively, in line with the ionic character of the Mg–C and Li–C interactions. Slightly bent bond paths and associated bond critical points (BCPs) for these interactions can be readily identified, along with corresponding ring critical points (RCPs) located within each of the four-membered ring motifs enclosed by the Mg–C and Li–C bond paths (Fig. 2). The BCPs are located closer to the positively charged Mg^{2+} and Li^+ centres, correlating with their smaller bonding radius compared to that of the carbanion centres. The descriptors associated with each BCP also support a closed-shell ionic bonding regime, reflected in the small electron density $\rho(r)$ of ∼0.04 a.u. and small positive Laplacian $\nabla^2\rho(r)$ of ∼0.17 a.u. The Cremer/Kraka local energy density $H(r) = G(r) + V(r)$[17] at the BCP and the ratio $G(r)/\rho(r)$[18] (see SI) are also consistent with this assignment.

In **1**, the QTAIM charges on Li(TMEDA) fragments remain unchanged, while Mn(II) has an assigned charge (+1.1*e*) well below its formal oxidation state. In combination with those associated with the carbon centres (−0.42*e*), this indicates more dative bonding in **1**. This is also borne out in the associated parameters of the Mn–C BCPs ($\rho(r)$ = 0.07 a.u., $\nabla^2\rho(r)$ ∼0.14 a.u.), with the energy density ($H(r)$ = −0.02 a.u.) now being slightly negative. It is also noteworthy that the BCPs are located closer to the midpoint of the Mn–C bond path. NBO analysis of the donor/acceptor interactions confirms donations from the bridging C-donor into the vacant β-spin 3d and 4s acceptor orbitals on Mn, with corresponding $E^{(2)}$ of 8.3, 13.9 and 18.4 kcal mol^{-1}. Combined with the LP(C) → Mn(4s) interaction within the α-manifold ($E^{(2)}$ = 15.5 kcal mol^{-1}), this results in an overall stronger donation towards the Mn centre than in the Mg congener and correlates with stronger C → Mn dative character. On the other hand, the donation into the Li^+ is only marginally larger than found in **1**, attributable to shorter Li···C distances.

Complementing solid state studies, solution state studies of **1** and **2** offered further insights. The most notable feature in ^{1}H NMR spectrum of **2** in C_6D_6 is the M-CH_2 resonance observed at −0.53 ppm upfield shifted relative to $^n Bu_2Mg$, while the ^{7}Li NMR spectrum displays a single sharp resonance at 1.21 ppm.

Resonances belonging to the TMEDA donor suggest that the ligand stays coordinated on the Li centres, which is in line with closely related [$(TMEDA)_2Li_2Mg(CH_2SiMe_3)_4$].[14] This is further supported by ^{1}H NMR DOSY study. Employing method developed by Stalke,[19] in C_6D_6 **2** has an estimated molecular weight of 459 g mol^{-1} which is in good agreement with the structure observed in the solid state (+8% error). ^{1}H NMR spectrum of **1** in C_6D_6 displays three highly broadened, and paramagnetically shifted resonances centred at −4.15, 2.81 and 9.90 ppm.

Evans method analysis[20] of **1** in C_6D_6 reveals $\mu_{eff} = 5.93\mu_B$ which is in excellent agreement with the theoretical value for high-spin (S = 5/2) Mn(II) and in good agreement with the one reported by Girolami.[4] Paramagnetic ^{7}Li NMR spectrum[21] shows two broad signals in C_6D_6 at 2.1 and 0.8 ppm, while in THF a single broad resonance is observed at 1.8 ppm.

Both **1** and **2** show limited stability in solutions. For **1** this was first observed with a steady decrease in the value of μ_{eff}, accompanied with gradual appearance of new diamagnetic resonances. Spectra of **2**, revealed formation of butane evidenced by two multiplets at 1.22 and 0.85 ppm in a 2 : 3 ratio, accompanied with the loss of sharp singlet resonances of TMEDA and appearance of multiple resonances in the region around −0.5 ppm. Despite not being able to accurately identify any of the newly formed decomposition products (^{7}Li NMR spectrum shows four resonances implying presence of multiple species), we propose that the anionic ate activation enhances the reactivity of ^{n}Bu groups which due to the proximity constraint α-metalate TMEDA ligand(s). Metalation of TMEDA is known to happen with Li bases or bimetallic mixtures.[22] By comparison, although β-hydride elimination in **1** cannot be ruled out, ^{1}H spectra of **1** also show resonances attributed to butane formation consistent with the manganate acting as a base.

With a good understanding of the constitution of **1** and **2**, we next decided to compare their catalytic ability in hydroamination of styrene using piperidine as a model substrate. With 10 mol% of **1** in C_6H_6 at room temperature (Scheme 1), anti-Markovnikov hydroamination product 1-(phenylethyl)piperidine (**3a**) was obtained in 69% yield after only 15 min, which increased to 84% after 18 h reaction time (Scheme 1). However, using the Mg congener **2**, the same product **3a** was obtained in lower yields of 52% and 73% after 15 min and 18 h, respectively. Performing the reaction in coordinating THF solvent had a detrimental effect, but again **1** outperformed **2** (see SI for details). Focusing solely on **1**, heating the reaction had no effect on the yield, while decreasing the catalyst loading slowed down the reaction with 5 mol% and 1 mol% of **1** affording only 40% and 17% of **3a**, respectively after 15 min, which would reach completion after prolonged reaction times.

Previous studies in s-block catalysed hydroamination have suggested that these reactions proceed through formation of nucleophilic metal amide, followed by the substrate insertion into the M–N bond.[8] To probe this pathway we conducted a series of stoichiometric studies. NMR studies revealed that both **1** and **2** rapidly deprotonate piperidine affording amido species accompanied by liberation of butane (Scheme 2(i)). Cooling pentane solutions to −30 °C deposited colourless crystals of $[(TMEDA)_2Li_2M(NC_5H_{10})_4]$ (M = Mn (**4**); Mg (**5**)). SCXRD studies revealed that **4** and **5** adopt the classical "Weiss motif" comparable to **1** and **2**, with centrally positioned M(II)

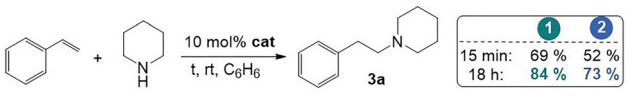

Scheme 1 Hydroamination of styrene with piperidine using **1** and **2** as catalysts. NMR yield determined using ferrocene as the internal standard.

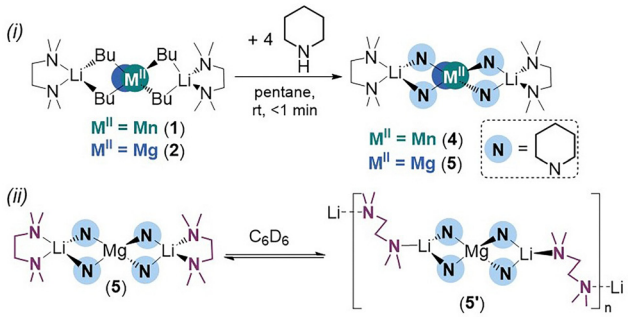

Scheme 2 (i) Synthesis of **4** and **5**. (ii) Proposed equilibrium of **5** and **5′** in C_6D_6 solution.

connected to outer TMEDA-solvated Li cations by four piperidide bridges. Closely related structures have been previously found in sodium magnesiate $[(TMEDA)_2Na_2Mg(NC_5H_{10})_4]$[9] and lithium manganate $[(TMEDA)_2Li_2Mn\{N(H)Mes\}_4]$.[7]

While rapid decomposition of **4** under vacuum precluded its isolation, full NMR spectroscopic characterisation of **5** was conducted. Most notably the ^{7}Li NMR spectrum shows two resonances in C_6D_6 at 0.49 and 1.37 ppm, while ^{1}H and ^{13}C NMR spectra showed only one set of broadened resonances for piperidide, and TMEDA ligands. However, in d_8-THF a single resonance in ^{7}Li NMR spectrum was observed at 0.55 ppm, while the resonances in ^{1}H and ^{13}C NMR spectra revealed free TMEDA.[23] We propose that in benzene solution **5** is in equilibrium with $[\{(TMEDA)Li_2Mg(NC_5H_{10})_4\}_\infty]$ (**5′**) where the TMEDA acts as a bridging ligand between neighbouring $\{Li_2MgBu_4\}$ cores (Scheme 2(ii)). Supporting this interpretation, deprotonation of diethylamine with **2** led to isolation and structural characterisation of $[\{(TMEDA)Li_2Mg(NEt_2)_4\}_\infty]$ (**6′**) with δ_{Li} = 1.38 ppm.

Considering immediate formation and analogous structures of **4** and **5**, we expected that the following insertion of vinylarene in the bimetallic amide to form alkyl manganate and magnesiate would explain the better efficiency of **1**. Unfortunately, we were not able to isolate or even observe such species, and under stoichiometric conditions only metal amide and the final product were identified. Based on the bonding analysis of **1** and **2**, we would tentatively speculate that the greater ability of Mn(II) centre to accept electron density in its orbitals can help with the insertion step.

We finished our study by exploring the substrate scope of intermolecular hydroamination catalysed by **1** and found that both with electron withdrawing (Br, Cl, F) and donating (^{t}Bu, OMe) substituted styrenes good yields (46–77%, Fig. 3) can be achieved, however electron rich systems require longer reaction times. Interestingly, sodium ferrates showed the opposite trend, with electron rich substituents affording better outcomes.[24] Greater steric hindrance has a detrimental effect, with diphenylethylene affording 55% of hydroaminated product after 18 h, and α-styrene only 11%. Different amines were also probed, and we observed that further enhancing nucleophilicity of amine has a detrimental effect with morpholine and diethylamine affording 61% and 21% of hydroaminated product after 18 h, respectively, while diisopropylamine and dicyclohexylamine afforded no product under tested conditions. However, significant decrease in

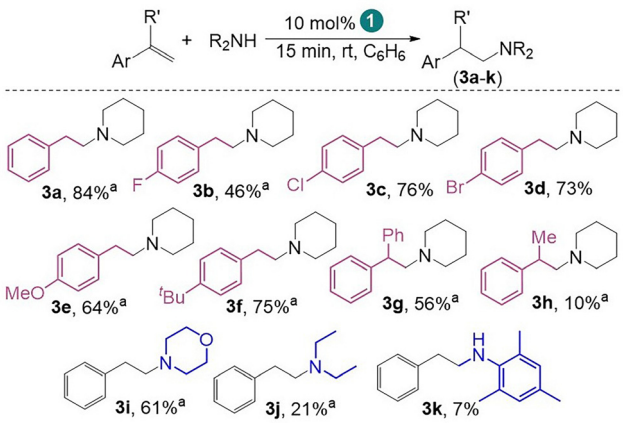

Fig. 3 Hydroamination of styrene derivatives with selected amines. Conditions: vinylarene (0.2 mmol), amine (0.25 mmol), **1** (0.02 mmol), C_6H_6 (0.5 mL), rt, 15 min. NMR yield determined using ferrocene as the internal standard. (a) Reaction performed for 18 h.

the nucleophilicity of amine is also unfavourable, with primary amine such as 2,4,6-trimethylaniline affording only 7% of hydroaminated product.

In conclusion, we successfully isolated and structurally characterised previously elusive lithium tetra(*n*-butyl) manganate(II) and magnesiate. Solid state characterisation shows the two compounds to be isomorphous, while the DFT calculations indicate that there is a greater covalent character contribution in C–Mn than in the C–Mg bond. Powered by anionic ate activation both complexes can serve as pre-catalysts for hydroamination of styrene *via* nucleophilic bimetallic amides. Under the tested conditions, manganate shows slightly better activity possibly due to Mn centre contributing to activation of the olefin. However, it is possible that manganate allows other type of activation accessible to transition metals. Further studies are under way in our laboratory.

We thank Royal Society (University Research Fellowship to M. U.) and University of Bath (PhD studentship to R. S. J) for their generous funding of this research. We thank Dr John P. Lowe for his assistance with NMR experiments. We acknowledge the Irish Centre for High-End Computing (ICHEC) and LuxProvide for the provision of HPC facilities (MeluXina) and technical support.

Conflicts of interest

There are no conflicts to declare.

Data availability

The data that supports the findings of this study are available in the supplementary material of this article. Supplementary Information: Synthetic procedures, structural and spectroscopic data, and calculations details.

CCDC 2474583–2474587 contains the supplementary crystallographic data for this paper.[25a–e]

Notes and references

1 (*a*) H. Gilman and J. C. Bailie, *J. Org. Chem.*, 1937, **2**, 84; (*b*) H. Gilman and R. H. Kirby, *J. Am. Chem. Soc.*, 1941, **63**, 2046.
2 (*a*) G. Wilkinson, F. A. Cotton and J. M. Birmingham, *J. Inorg. Nucl. Chem.*, 1956, **2**, 95; (*b*) W. Bunder and E. Weiss, *Z. Naturforsch., B: Chem. Sci.*, 1978, **33**, 1235.
3 (*a*) G. Cahiez, C. Duplais and J. Buendia, *Chem. Rev.*, 2009, **109**, 1434; (*b*) R. A. Layfield, *Chem. Soc. Rev.*, 2008, **37**, 1098.
4 R. J. Morris and G. S. Girolami, *Organometallics*, 1989, **8**, 1478.
5 J. Garcia-Alvarez, A. R. Kennedy, J. Klett and R. E. Mulvey, *Angew. Chem., Int. Ed.*, 2007, **46**, 1105.
6 M. Uzelac, P. Mastropierro, M. de Tullio, I. Borilovic, M. Tarres, A. R. Kennedy, G. Aromi and E. Hevia, *Angew. Chem., Int. Ed.*, 2021, **60**, 3247.
7 R. S. Jones, M. F. Mahon and M. Uzelac, *Eur. J. Inorg. Chem.*, 2024, **27**, e202400512.
8 (*a*) M. R. Crimmin, M. Arrowsmith, A. G. M. Barrett, I. J. Casely, M. S. Hill and P. A. Procopiou, *J. Am. Chem. Soc.*, 2009, **131**, 9670; (*b*) J. F. Dunne, D. B. Fulton, A. Ellern and A. D. Sadow, *J. Am. Chem. Soc.*, 2010, **132**, 17680.
9 (*a*) X. Zhang, T. J. Emge and K. C. Hultzsch, *Angew. Chem., Int. Ed.*, 2012, **51**, 394; (*b*) L. Davin, A. Hernan-Gomez, C. McLaughlin, A. R. Kennedy, R. McLellan and E. Hevia, *Dalton Trans.*, 2019, **48**, 8122; (*c*) C. Gallegos, R. Camacho, M. Valiente, T. Cuenca and J. Cano, *Catal. Sci. Technol.*, 2016, **6**, 5134.
10 (*a*) R. E. Mulvey, *Acc. Chem. Res.*, 2009, **42**, 743; (*b*) D. R. Armstrong, E. Brammer, T. Cadenbach, E. Hevia and A. R. Kennedy, *Organometallics*, 2013, **32**, 480.
11 A. Torres-Calis and J. J. García, *ACS Omega*, 2022, **7**, 37008.
12 B. Cui, Y. Zheng, H. Sun, H. Shang, M. Du, Y. Shang and C. T. Yavuz, *Nat. Commun.*, 2024, **15**, 6647.
13 T. Greiser, J. Kopf, D. Thoennes and E. Weiss, *Chem. Ber.*, 1981, **114**, 209.
14 S. E. Baillie, W. Clegg, P. Garcia-Alvarez, E. Hevia, A. R. Kennedy, J. Klett and L. Russo, *Organometallics*, 2012, **31**, 5131.
15 P. Pyykko, *J. Phys. Chem. A*, 2015, **119**, 2326.
16 G. S. Girolami, C. G. Howard, G. Wilkinson, H. M. Dawes, M. Thornton-Pett, M. Motevalli and M. B. Hursthouse, *J. Chem. Soc., Dalton Trans.*, 1985, 921.
17 D. Cremer and E. Kraka, *Croat. Chem. Acta*, 1983, **57**, 1259.
18 R. F. W. Bader and H. Essén, *J. Chem. Phys.*, 1984, **80**, 1943.
19 R. Neufeld and D. Stalke, *Chem. Sci.*, 2015, **6**, 3354.
20 D. P. Shoemaker, C. W. Garland and J. W. Nibler, *Experiments in Physical Chemistry*, 5th edn, McGraw-Hill: New York, 1989.
21 Previously ^{7}Li resonances of **1** were not observed, but further adjustments of experimental parameters can allow observation of these. See SI for details.
22 (*a*) F. H. Köhler, N. Hertkorn and J. Blümel, *J. Chem. Ber.*, 1987, **120**, 2081; (*b*) S. Harder and M. Lutz, *Organometallics*, 1994, **13**, 5173; (*c*) A. Hildebrand, P. Lonnecke, L. Silaghi-Dumitrescu, I. Silaghi-Dumitrescu and E. Hey-Hawkins, *Dalton Trans.*, 2006, 967; (*d*) B. Conway, J. Garcia-Alvarez, E. Hevia, A. R. Kennedy, R. E. Mulvey and S. D. Robertson, *Organometallics*, 2009, **28**, 6462.
23 A. R. Kennedy, J. Klett, C. T. O'Hara, R. E. Mulvey and G. M. Robertson, *Eur. J. Inorg. Chem.*, 2009, 5029.
24 A. Tortajada and E. Hevia, *ACS Org. Inorg. Au*, 2025, **5**, 62.
25 (*a*) R. S. Jones, T. Krämer, G. S. Nichol, M. F. Mahon, J. G. C. Kragskow and M. Uzelac, CCDC 2474583: Experimental Crystal Structure Determination, 2025, DOI: 10.5517/ccdc.csd.cc2p2082; (*b*) R. S. Jones, T. Krämer, G. S. Nichol, M. F. Mahon, J. G. C. Kragskow and M. Uzelac, CCDC 2474584: Experimental Crystal Structure Determination, 2025, DOI: 10.5517/ccdc.csd.cc2p2093; (*c*) R. S. Jones, T. Krämer, G. S. Nichol, M. F. Mahon, J. G. C. Kragskow and M. Uzelac, CCDC 2474585: Experimental Crystal Structure Determination, 2025, DOI: 10.5517/ccdc.csd.cc2p20b4; (*d*) R. S. Jones, T. Krämer, G. S. Nichol, M. F. Mahon, J. G. C. Kragskow and M. Uzelac, CCDC 2474586: Experimental Crystal Structure Determination, 2025, DOI: 10.5517/ccdc.csd.cc2p20c5; (*e*) R. S. Jones, T. Krämer, G. S. Nichol, M. F. Mahon, J. G. C. Kragskow and M. Uzelac, CCDC 2474587: Experimental Crystal Structure Determination, 2025, DOI: 10.5517/ccdc.csd.cc2p20d6.